

Article

Load Characteristics and Extreme Response of Straight-Bladed Floating VAWT Using a Fully Coupled Model

Wenping Luo ^{1,2}, Weiqin Liu ^{1,2,*}, Meng Yang ³, Shuo Chen ², Xuemin Song ^{1,2} and Weiguo Wu ⁴

¹ Key Laboratory of High Performance Ship Technology, Wuhan University of Technology, Ministry of Education, Wuhan 430063, China

² Department of Naval Architecture and Ocean Engineering, School of Naval Architecture, Ocean and Energy Power Engineering, Wuhan University of Technology, Wuhan 430063, China

³ China Ship Design and Research Center, Wuhan 430060, China

⁴ Green & Smart River-Sea-Going Ship, Cruise and Yacht Research Centre, Wuhan University of Technology, Wuhan 430063, China

* Correspondence: liuweiqin_123@sina.com

Abstract: Operating Offshore Floating Vertical Axis Wind Turbines (OF-VAWT) have the potential to perform well in the deep-sea area. Some researchers gave performance prediction by developing simplified computing models. However, these models have imperfections in considering load and motion nonlinearity, especially in extreme environments. In this work, a numerical model is developed composed of Computational Fluid Dynamics (CFD) and Dynamic Fluid Body Interaction (DFBI) to acquire the aero-hydrodynamic load and performance of OF-VAWT in general and extreme environments. Unsteady Reynolds-Averaged Navier-Stokes (URANS), SST k- ω and Eulerian Multi-Phase (EMP) models are combined to generate a gas-liquid two-phase flow field; the Volume of Fluid (VOF) model is employed to capture free-surface and make numerical wind-wave. DFBI superposition motion technology is proposed for local motion definition and motion solution, and overset with sliding meshes is introduced to achieve the grid motion. The numerical approach is verified by the tunnel and tank experimental data from the available literature. Simulation results of general cases, such as variable wind speed, wave height and wave length, are compared to discuss the effect of environmental parameters on load and performance. Comparison shows that this straight-bladed OF-VAWT is more susceptible to wind speed. Furthermore, the aerodynamic load generated by the shut-down rotor is still significant in extreme environment, which has implications for the development of OF-VAWT controller.

Keywords: vertical axis wind turbine; semi-submersible; wind-wave coupling; computational fluid dynamics; aero-hydrodynamics; extreme environment



Citation: Luo, W.; Liu, W.; Yang, M.; Chen, S.; Song, X.; Wu, W. Load Characteristics and Extreme Response of Straight-Bladed Floating VAWT Using a Fully Coupled Model. *J. Mar. Sci. Eng.* **2023**, *11*, 185. <https://doi.org/10.3390/jmse11010185>

Academic Editors: Galih Bangsa and Martin Otto Laver Hansen

Received: 25 November 2022

Revised: 29 December 2022

Accepted: 30 December 2022

Published: 11 January 2023



Copyright: © 2023 by the authors. Licensee MDPI, Basel, Switzerland. This article is an open access article distributed under the terms and conditions of the Creative Commons Attribution (CC BY) license (<https://creativecommons.org/licenses/by/4.0/>).

1. Introduction

Wind energy exploration is a popular research topic in recent years, as it can be harnessed without carbon emission to handle environmental problems. Recently, wind power development has turned its sight from onshore to offshore [1], and coastal fixed-type wind turbines are the beginning. Furthermore, it is well-known that most of the wind energy is far from the coast, so utilizing energy in deep-sea areas interests various scholars and countries today.

Floating Offshore Wind Turbines (FOWT) in which the buoyancy is provided by a floating foundation and the power is generated by a rotor are generally classified as Vertical Axis Wind Turbines (VAWT) and Horizontal Axis Wind Turbines (HAWT) according to the direction of the rotating axis [2]. In addition, the semi-submersible platform with a larger platform is proved to be a better choice for offshore wind turbines in Offshore Code Comparison Collaboration Continuation (OC4) [3]. Further, it is also known the VAWT could capture wind energy in all directions without a steering device, and its nacelle and

gearbox are closer to the bottom. Accordingly, the combination of a semi-submersible platform and VAWT is expected to perform well in the deep-sea environment to avoid common damage [4].

Operating Offshore Floating Vertical Axis Wind Turbines (OF-VAWT) can be greatly influenced by the environment. Attentionally, enormous wind turbines are susceptible to being damaged by wind loads. In 2008, five coastal land-based wind turbines in Taiwan were destroyed by super typhoon ‘Jangmi’ [5], and more than 18 wind turbines were damaged during typhoon ‘Weimaxun’ in 2014 [6]. Additionally, numerous offshore floating structures are capsized or damaged by wave load. In 2013, ‘Prestige’ was damaged during an encounter with a large wave [7], and in 2022 a large ship named ‘ALSALMY6’ capsized due to heavy weather conditions in the Persian Gulf. Therefore, it is essential to investigate the load and motion response of OF-VAWT in both general and extreme environments for engineering design implications.

Operating offshore wind turbines generally suffer from aero-hydrodynamic coupling in wind-wave environments. Recently, some scholars made efforts on predicting the performance of several FOWTs considering aero-hydrodynamic coupling, the properties including rotor, platform and simulation module are shown in Table 1. Obviously, floating HAWTs are the primary objects in current research, and OF-VAWTs are rarely investigated especially for the straight-bladed type. In addition, the semi-submersible platform DeepCWind is mostly employed as the floating foundation, and CFD technology is welcomed in solving aero-hydrodynamics simultaneously by more scholars. Some scholars also studied the coupling interaction by other simplified means. For instance, the floating foundation is assumed as a forced motion with regular function, through this way, the effect of pitch and surge motion on the aerodynamic performance of FOWT is investigated [8–10]. In a word, the effect of aero-hydrodynamic coupling on performance of straight-bladed OF-VAWT is rarely investigated especially in an extreme environment.

Table 1. Related efforts of FOWT considering aero-hydrodynamic coupling.

Author (Year)	Rotor	Platform	Aerodynamic Module	Hydrodynamic Module
Wu et al. (2016) [11]	NERL-5MW	Spar-type	CFD	CFD
Tran and Kim (2018) [12]	NERL-5MW	DeepCWind	CFD	CFD
Wang et al. (2018) [13]	NERL-5MW	Spar-type	BEM	Potential flow
Zhang and Kim (2018) [14]	NERL-5MW	DeepCWind	CFD	CFD
Guo et al. (2019) [15]	Φ -type	Spar-type	Streamtube	Potential flow
Cheng et al. (2019) [16]	NERL-5MW	DeepCWind	CFD	CFD
Li et al. (2020) [17]	NERL-5MW	DeepCWind	BEM	Potential flow
Gao et al. (2022) [18]	Darrieus-type	TLP-type	Vortex	Potential flow
Lee et al. (2022) [19]	Darrieus-type	TLP-type	Streamtube	Potential flow

Methodology for investigating the aero-hydrodynamics of OF-VAWTs includes model experiments and numerical simulations [20]. The experimental method is generally used for validation considering its high cost and restricted measurement, thus numerical simulation is more popular in analyzing details and conducting numerous cases. There are several computing codes developed for OF-VAWT in different research institutes. For instance, Tianjin University developed an aero-hydrodynamic code for Darrieus-spar type based on double-multiple-stream-tubes and potential theory [21], as well as the Simo-Riflex-DMS code presented by the Norwegian University of Science and Technology [22] and the Hawc2 code presented by the Technical University of Denmark [23]. However, since too many assumptions are introduced into Blade Element Momentum (BEM), Vortex model and potential theory, there are imperfections in considering nonlinear loads, such as dynamic stall, green water and slamming [24]. Therefore, it is essential to analyze the OF-VAWT using Computational Fluid Dynamics (CFD) that can meet the requirements of accuracy in both aerodynamics and hydrodynamics.

The effect of dreadful environments on FOWT has been investigated by scholars in several ways. However, the prediction of OF-VAWT, especially for the straight-bladed type, is rarely conducted, and most related research has imperfections in consideration of the load and motion nonlinearity due to the adopted simplified computing model. Therefore, the present study aims to investigate the aero-hydrodynamic load and performance characteristics of straight-bladed OF-VAWT in general and extreme environments. To consider the nonlinear aero-hydrodynamics simultaneously, the adopted CFD and Dynamic Fluid Body Interaction (DFBI) superposition motion technology are described in Section 2. We present the validation of this numerical approach, which was carried out by a VAWT wind tunnel experiment and a tank model experiment of free-decay motion, in Section 3. The details of straight-bladed OF-VAWT system, including geometry, properties and numerical model, are present in Section 4. In Section 5, we present several typical cases to analyze the characteristics of aero-hydrodynamic performance and load in time-domain. The differences in load and performance statistics between different environment cases, as well as implications for engineering design, are discussed in Section 6.

2. Numerical Methodology

It is well known that FOWT has complicated aero-hydrodynamic coupling load and multiple motions, thus, simulating the body motion and fluid load with high-fidelity are two keys. Further, the aforementioned CFD technology has advantages in solving nonlinear loads for both aerodynamics and hydrodynamics, and the mooring line could be performed by a quasi-static catenary model. Accordingly, the viscous-flow CFD model, quasi-static catenary model and DFBI superposition motion are combined to predict the aero-hydrodynamic load and performance of OF-VAWT in this paper.

2.1. Computational Fluid Dynamics

Various assumptions are added in traditional theory to simplify problems so that load nonlinearity of wind and wave is not considered. We employed aero-hydrodynamic solvers based on viscous-flow theory, as well as the finite volume method (FVM). The spatial fluid domain is discretized into small-scale control volumes with finite numbers, assuming that each control volume is governed by continuity and momentum equations. However, parameters such as velocity and pressure changed randomly over time, the fluid flow will be more complicated and difficult to solve. On account of accuracy and cost, Unsteady Reynolds-Averaged Navier Stokes (URANS) is mostly used to predict turbulent motion; the idea of RANS method is to average Navier-Stokes equations with time, decompose velocity and pressure into mean and perturbation; the RANS equation is described as follows:

$$\rho \left[\frac{\partial \bar{u}_i}{\partial t} + \frac{\partial (\overline{u_i u_j})}{\partial x_j} \right] = -\frac{\partial \bar{p}}{\partial x_i} + \mu \nabla^2 u_i + \frac{\partial}{\partial x_j} (-\rho \overline{u_i' u_j'}) \tag{1}$$

where u is velocity, ρ is density of fluid, p is press, μ is molecular viscosity, \bar{u} is average speed of time, \bar{p} is average press of time, $(-\rho \overline{u_i' u_j'})$ is an item of Reynolds stress which is a second-order tensor. As new unknowns bring in, a turbulence model should be used to close the equations. Particularly, the approach combining the RANS equation and $k-\omega$ turbulence model has been validated in calculating aerodynamics and hydrodynamics [8,25]. Transport equations of turbulent kinetic energy and dissipation rate for SST $k-\omega$ model are described as follows:

$$\frac{\partial}{\partial t} (\rho k) + \frac{\partial}{\partial x_i} (\rho k u_i) = \frac{\partial}{\partial x_j} \left(\left(\mu + \frac{\mu_t}{\sigma_k} \right) \frac{\partial k}{\partial x_j} \right) + \widetilde{G}_k - Y_k + S_k \tag{2}$$

$$\frac{\partial}{\partial t} (\rho \omega) + \frac{\partial}{\partial x_i} (\rho \omega u_i) = \frac{\partial}{\partial x_j} \left(\left(\mu + \frac{\mu_t}{\sigma_\omega} \right) \frac{\partial \omega}{\partial x_j} \right) + G_\omega - Y_\omega + D_\omega + S_\omega \tag{3}$$

where \widetilde{G}_k is a term of turbulent kinetic energy generation for k , G_ω is a term of dissipation rate generation, D_ω is a term of cross diffusion for ω , Y_k is a term of turbulent kinetic energy

dissipation for k , Y_ω is a term of turbulent kinetic energy dissipation for ω , S_k and S_ω are user-defined terms. Then, the basic solution of the flow field can be obtained by combining Equations (1)–(3). To capture the gas-liquid two-phase interface precisely, Volume of Fluid (VOF) is adopted in which a phase volume fraction is used to ascertain phase distribution and location of interface, which is defined as follows:

$$a_i = \frac{V_i}{V} \tag{4}$$

where V_i is volume of phase i in the mesh element, V is volume of mesh element. The sum of the volume fractions of all phases in an element must be one. According to the value of volume fraction, the existence of different phases or fluids in grid cells can be distinguished. $a_i = 0$ means that the corresponding mesh element has no phase at all, $a_i = 1$ means that the corresponding mesh element is completely phase filled, $0 < a_i < 1$ means that there are interfaces of multiple phases.

2.2. DFBI Superposition Motion

Different from the conventional offshore structures, the OF-VAWT has 7-DOF motion, including global 6-DOF free motion and local 1-DOF rotational motion. Attentionally, this local rotate motion is a superposition motion based on global motion. However, the conventional motion equation can only contain 6-DOF, thus this paper intends to decouple the composite motions by defining the relationship between the global coordinate system and the rotating coordinate system. First, the rotor and the platform are integrated as one body to solve the 6-DOF motion. The overall structure generates three translational motions and three rotational motions based on the global coordinate system, and the equations are shown as follows.

$$m \frac{dv}{dt} = F \tag{5}$$

$$I \frac{d\omega}{dt} + \omega \times I\omega = M \tag{6}$$

where m is the mass of body, F is the resultant force acting on the body, and v is the velocity. Furthermore, ω is the angular velocity, M is the resultant bending moment, and I is the tensor of the moments of inertia. Gravity and fluid forces are the main external effects except for special conditions. The fluid force F_{fluid} , moment M_{fluid} and moment of inertia I are calculated by the following formula:

$$I = \begin{bmatrix} I_{xx} & I_{xy} & I_{xz} \\ I_{xy} & I_{yy} & I_{yz} \\ I_{xz} & I_{yz} & I_{zz} \end{bmatrix} \tag{7}$$

$$F_{fluid} = \sum_{i=1}^A p_i \cdot \vec{n}_i + \sum_{i=1}^A \tau_i \cdot \vec{v}_i \tag{8}$$

$$M_{fluid} = \sum_{i=1}^A l_i \cdot p_i \cdot \vec{n}_i + \sum_{i=1}^A l_i \cdot \tau_i \cdot \vec{v}_i \tag{9}$$

where I_{ii} represents principal components along the diagonal and I_{ij} represents off-diagonal components. p_i and τ_i are, respectively, the pressure and shear stress acting on face i , \vec{n}_i and \vec{v}_i are the area vector of face, l_i is the distance vector from the body center of mass to the center of face, A represents the entire body surface area. Figure 1 illustrates the relationship

between the local coordinate system and the global coordinate system, so the translation and rotation of the rotating coordinate system can be formulated as follows:

$$\begin{pmatrix} d\theta_{lx} \\ d\theta_{ly} \\ d\theta_{lz} \end{pmatrix} = \begin{pmatrix} d\theta_{gx} \\ d\theta_{gy} \\ d\theta_{gz} \end{pmatrix} \tag{10}$$

$$\begin{pmatrix} dX_l \\ dY_l \\ dZ_l \end{pmatrix} = \begin{pmatrix} dX_g + L \sin d\theta_y \\ dY_g + L \cos d\theta_y \\ dZ_g + L(2 - \cos d\theta_x - \cos d\theta_y) \end{pmatrix} \tag{11}$$

where dX , dY , and dZ represent the tiny translation distance in the three directions, and $d\theta_i$ represents the tiny rotation angle about the three main axes, subscript l represents local coordinate system (rotation system), and subscript g means global coordinate system. Finally, the Z -axis of the local coordinate system is set as the rotation axis with constant angular speed.

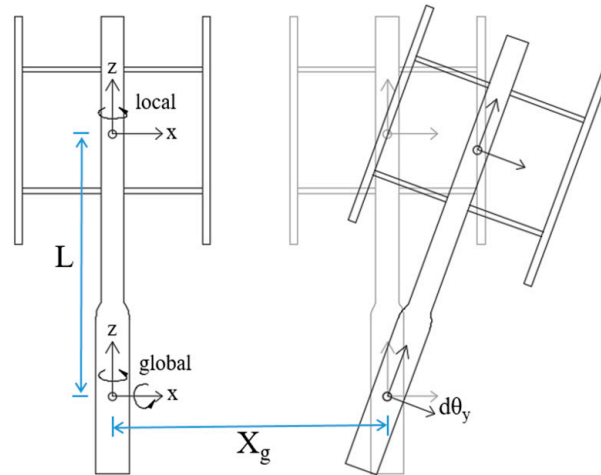


Figure 1. Definition of local and global coordinates in superposition motion.

2.3. Mooring Model

The mooring lines in FOWT systems, subjected to their own weight, are hanging between two points (anchors and fairleads). To consider the effect of a mooring system on hydrodynamics and motion, a quasi-static catenary model is employed. Figure 2 illustrates the forces and curve. The shape can be defined as follows:

$$x = \frac{c}{\lambda_0 g} u + \frac{c^2}{DL_{eq} \lambda_0 g} \sinh(u) + \alpha \tag{12}$$

$$y = \frac{c}{\lambda_0 g} \cosh(u) + \frac{c^2}{2DL_{eq} \lambda_0 g} \sinh^2(u) + \beta \tag{13}$$

$$c = \frac{\lambda_0 L_{eq} g}{\sinh(u_2) - \sinh(u_1)} \tag{14}$$

where g is the gravity acceleration, λ_0 and L_{eq} are the mass per unit length and relaxation length of the catenary, respectively. D is the stiffness of catenary, α and β are integration constants depending on the position of the two end points and the total catenary mass, u is related to inclination angle ϕ as follows:

$$\tan \phi = \sinh(u) \tag{15}$$

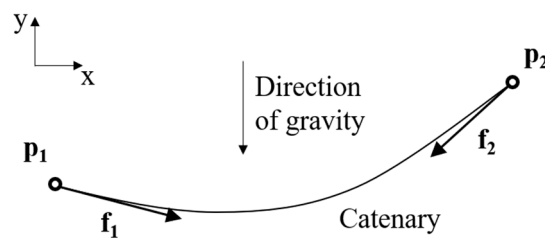


Figure 2. Force analysis of a mooring line in quasi-static catenary model.

The parameter values u_1 and u_2 represent the positions of the catenary end points p_1 and p_2 in parameter space. Furthermore, the force f_1 and f_2 acting on the two end points can be expressed by u_1 and u_2 .

$$f_{1,x} = c, \quad f_{1,y} = c \sinh(u_1) \tag{16}$$

$$f_{2,x} = -c, \quad f_{2,y} = -c \sinh(u_2) \tag{17}$$

2.4. Coupling Scheme of Aero-Hydrodynamics

CFD technology and catenary model are employed to acquire fluid load and mooring load, respectively, and using the DFBI superposition motion approach to predict the body dynamic responses; thus, a coupling scheme is required to simulate dynamic responses of OF-VAWT in wind-wave environment, and the relationship between each module is shown in Figure 3. In the aerodynamic module, creating the rotate and air domain according to rotor geometry and discretizing them based on FVM, particularly, rotate motion is achieved by using sliding mesh. By importing wind field, the aerodynamic solution is completed by solving URANS equation. In addition, the procedure for creating, discretizing and solution in hydrodynamic module is similar to aerodynamic module, except for importing wave and current rather than wind field, and overset mesh is used to adapt free motion. Among them, Eulerian Multi-Phase (EMP) flow and VOF theory are employed to create gas-fluid two-phase flow and capture the interface precisely, respectively, so that air and water domains are combined together. For the dynamic module, six-degree system motion could be obtained by importing the aero-hydro-mooring dynamic load and moment of inertia into DFBI equation, and single-degree rotate motion is further achieved based on superposition motion method. Finally, the dynamic responses calculated, such as displacement, velocity, angle, and position, are returned to aerodynamic, hydrodynamic and mooring modules to conduct the next-step solution.

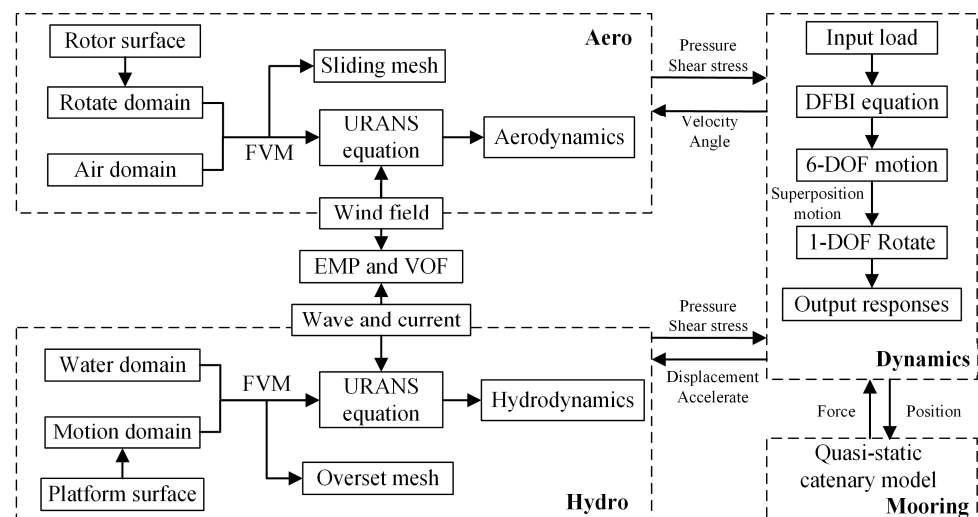


Figure 3. Coupling scheme and modules in this fully coupled model.

3. Validation of Numerical Approach

The accuracy of present numerical approach considering aero-hydrodynamic coupling needs to be validated by model experiments. However, there are rare model tests for straight-bladed OF-VAWT in wind-wave coupled environments, thus verifying the aerodynamic and hydrodynamic modules separately is common for scholars [16].

3.1. Aerodynamic Validation

A suitable and available research containing a three-blade vertical axis wind turbine experiment is supposed to verify the present aerodynamic module. Maeda et al. [26] conducted an aerodynamic model experiment of straight-bladed VAWT to investigate the effect of number of blades on aerodynamic performance. (see Figure 4a) A rotor with a radius of 1 m and a height of 1.2 m is selected as the experimental object, and NACA0021 is chosen as its airfoil section with a chord length of 0.265 m, the number of blades is 3. The power for different tip speed ratios (TSR) was measured in an 8 m/s uniform flow. Furthermore, some scholars have raised numerical research for this experiment based on the improved delayed detached eddy simulation (IDDES) model [9], so the experimental data, the IDDES model data and the present model data are compared in the following parts.

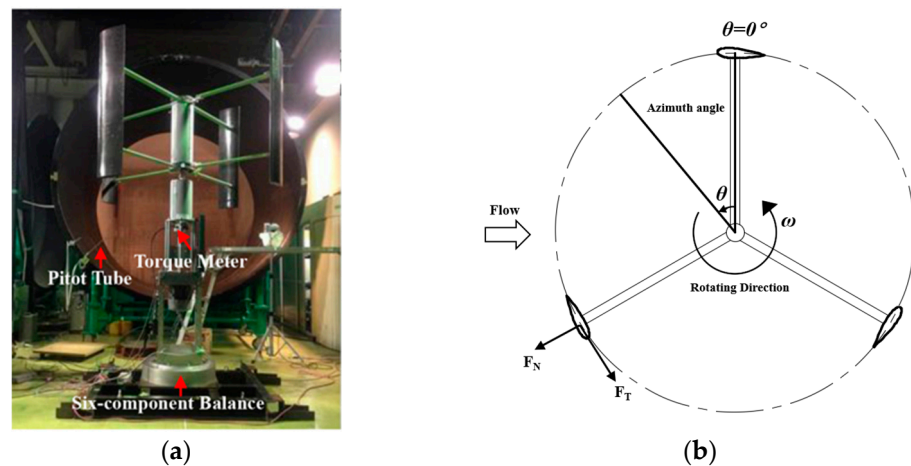


Figure 4. Aerodynamic experiment of a VAWT: (a) Testing arrangement (reproduced from [26], with permission from Elsevier, 2022) (b) Parameters in rotation.

Attentionally, Figure 4b illustrates that the incidence angle of airfoil is determined by wind and angular velocity, so the dimensionless parameter *TSR* is used as a criterion in the study of aerodynamic loads and performance (see Equation (18)). Furthermore, wind turbines are developed to utilize wind energy so that generated power coefficient C_p is a significant index to evaluate the quality, as shown in Equation (19).

$$TSR = \frac{\omega R}{U_0} \tag{18}$$

$$C_p = \frac{P}{0.5\rho AU_0^3} = \frac{Q\omega}{0.5\rho DHU_0^3} \tag{19}$$

where ω represents the rotating angular speed of blades, R is the radius, and U_0 is the incoming flow speed. ρ is the density of air. Swept wind area A is equal to the product of height H and diameter D , and power P is equal to the torque Q multiplied by the angular velocity ω .

The power coefficient C_p with different *TSR* of the experiment, IDDES model and present work are compared in Figure 5a, and it is obvious that the trend of these three results is close. However, numerical solution is completed in the ideal environment rather than the experimental environment. This may be a major reason why the numerical results

of the present study and IDDES model are slightly larger than the experimental values. To further investigate the period variation of the blade, the power coefficient C_p of single blade at the best TSR of 1.78 is shown in Figure 5b. Similarly, the results of the present study and IDDES are identical, and both them match well with the experiment.

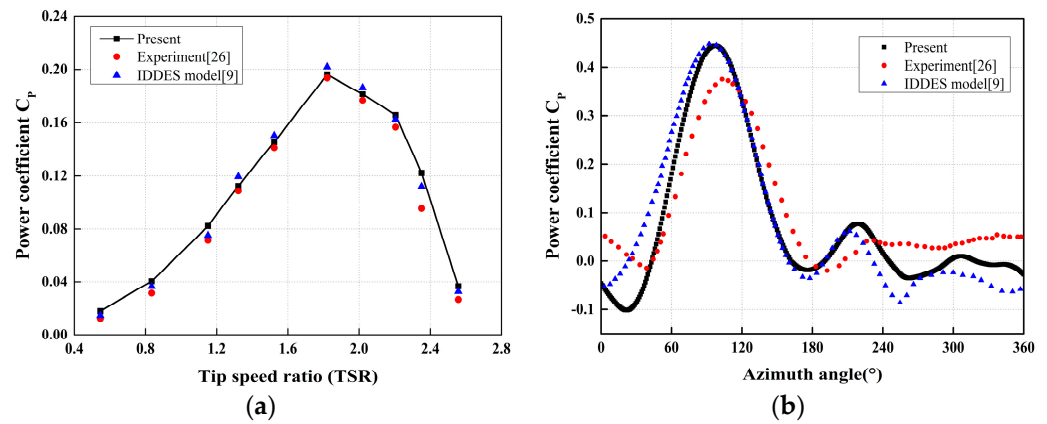


Figure 5. Comparison aerodynamic data of simulation against experiment: (a) Power coefficient against TSR (b) Power coefficient against azimuth angle [9,26]

3.2. Hydrodynamic Validation

To verify the hydrodynamic module, a tank experiment containing a submersible platform is required. The Offshore Code Comparison Collaboration Continuation (OC4) project, led by the National Renewable Energy Laboratory (NREL), is pretty influential in the wind energy field and carried out a tank test for FOWT floating foundation. Among them, free-decay motion is selected to validate the present hydrodynamic module in this section.

DeepCWind is in a great performance and popular in related research of FOWT. Over the years, many hydrodynamic numerical simulations have been carried out by scholars with different methods based on this platform. Coulling et al. [27] and Tran [28] compared the results of model tests and different versions FAST code. The hydrodynamic analysis of this platform was carried out by Luan et al. [29] based on the traditional potential flow theory. With the development of computer science, CFD technology is more often used for related research, such as commercial software STAR-CCM+ [30] and the open-source platform OpenFOAM [16].

Table 2 shows the calculated periods of free-decay motion including present study, previous related work and experiment. It can be seen that the proposed method in this paper matches well with the experiments and related simulations, and the comparison of pitch motion in free-decay is displayed in Figure 6. It is clear that the periodicity and amplitude of the results of several methods are relatively similar, although with slight differences. Overall, the present method of calculating hydrodynamic forces is effective.

Table 2. Period comparison of free decaying motion.

DOF	Exp [27]	Simo/Riflex [29]	Fast V8.1 [28]	Unsteady CFD [30]	naoe-FOAM-SJTU [16]	Present
Pitch	26.8	25.8	25.0	25.2	25.8	25.6
Roll	26.9	26.0	25.0	25.3	-	25.7
Heave	17.5	17.1	17.7	17.8	17.58	17.7

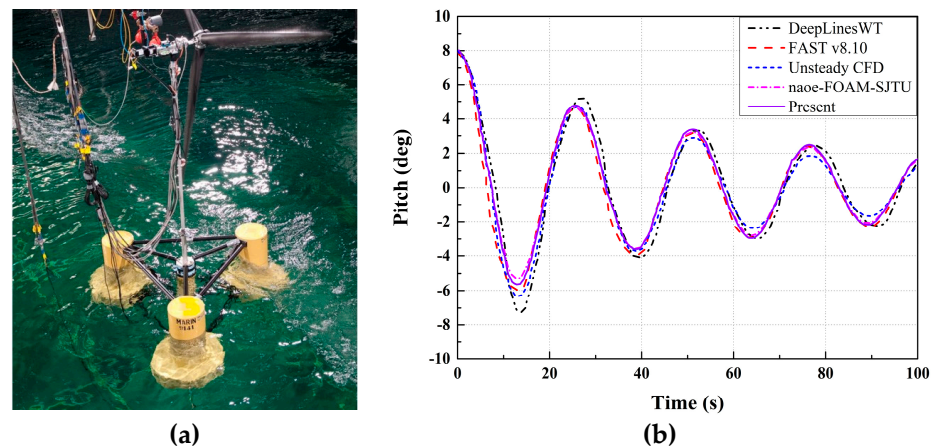


Figure 6. Comparison hydrodynamic data of simulation against experiment: (a) Testing arrangement (reproduced from [27], with permission from AIP Publishing, 2022) (b) Time-domain pitch curve of free–decay motion.

4. Model Description

4.1. OF-VAWT System

The floating vertical axis wind turbine is a hot candidate in deep-sea wind energy, a project is to design an OF-VAWT and place it in the South China Sea. Therefore, the impact of the ocean environment on this OF-VAWT needs to be taken into account in advance in this research. Wind and wave parameter settings are determined according to the environmental statistical report, and this selected full-scale floating wind turbine system is composed of a straight-bladed VAWT and a semi-submersible platform as shown in Figure 7a, and the information of properties is listed in Table 3.

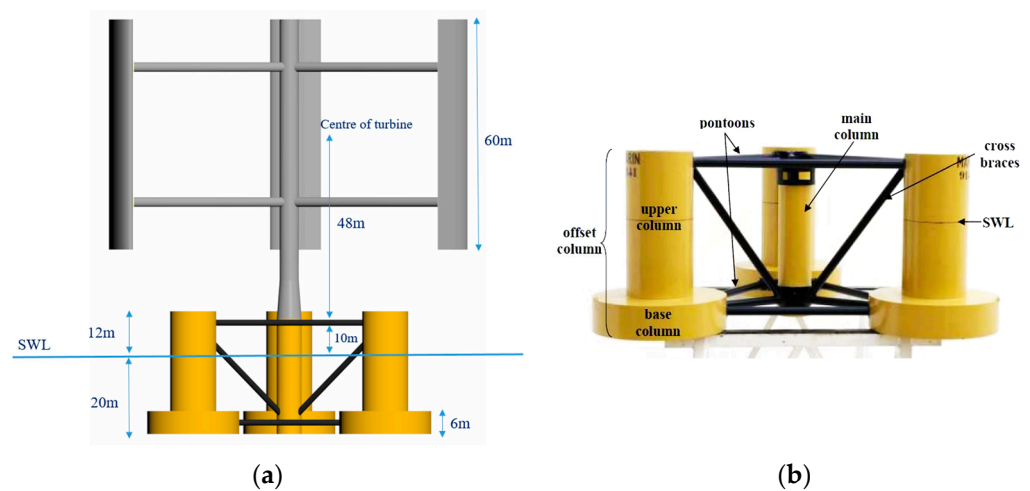


Figure 7. Geometric model of this OF-VAWT: (a) OF-VAWT system (b) OC4 foundation.

Table 3. Properties of this system.

Property	Parameter
Mass	1.37×10^7 kg
CM location below SWL	12.53 m
Total structure roll inertia bout CM	8.6×10^9 kg \times m ²
Total structure pitch inertia bout CM	8.6×10^9 kg \times m ²
Total structure yaw inertia bout CM	1.226×10^{10} kg \times m ²

4.2. Wind Turbine

The three blades showed good performance in terms of efficiency and noise in a model experiment [26], so this turbine is selected in this paper to combine a floating system. More detailed information about the full-scale rotor, including number of blades, airfoil section, radius and height, is described in Table 4.

Table 4. Wind turbine geometry.

Property	Parameter
Aerofoil section	NACA0021
Number of blades(<i>n</i>)	3
Length of chord(<i>c</i>)	13.25 m
Rotor diameter(<i>D</i>)	100 m
Height of straight-bladed(<i>H</i>)	60 m
Pitching angle(β)	8 deg
Height of center above main column	48 m

4.3. Floating Foundation

In recent years, spar-type floating platforms are often chosen in related research due to their good stability, but high mooring requirements and small platform area are the major drawbacks. However, the semi-submersible platform does not have these troubles and has been proven to have good performance [27]. A semi-submersible platform named DeepCWind belonging to the OC4 project is selected as the foundation of OF-VAWT. As shown in Figure 7b, one main column and three offset columns contribute to the buoyancy, and several braces are employed to connect each module. Detailed information for geometry is shown in Table 5. In addition, to restrict the displacement, three mooring lines are attached to platform, and properties of the corresponding mooring system refer to Cheng et al. [16].

Table 5. Floating foundation geometry.

Property	Parameter
Depth of platform base below SWL (total draft)	20 m
Elevation to platform top (tower base) above SWL	10 m
Distance between offset columns	50 m
Height of upper columns	26 m
Height of base columns	6 m
Diameter of main column	6.5 m
Diameter of offset (upper) column	12 m
Diameter of offset (bottom) column	24 m
Diameter of braces	1.6 m

4.4. Numerical Model of OF-VAWT

4.4.1. Computational Domain

The numerical model based on CFD in this paper is established in the STAR-CCM+ platform. As mentioned above (Section 2.3), the approach combining URANS with $k - \omega$ turbulence model is employed to govern fluid flow, creating the two-phase flow and capturing its interface by EMP and VOF, DFBI superposition motion is used to solve the dynamic motion response. Attentionally, establishing and discretizing a computational domain is the precondition of solution. Hence, several geometric regions, including background, overset and rotate domain, are created corresponding to numerical tank, system-body free motion and rotational motion (see Figure 8). Furthermore, volume and surface mesh generators are used to fill these domains with meshes based on FVM.

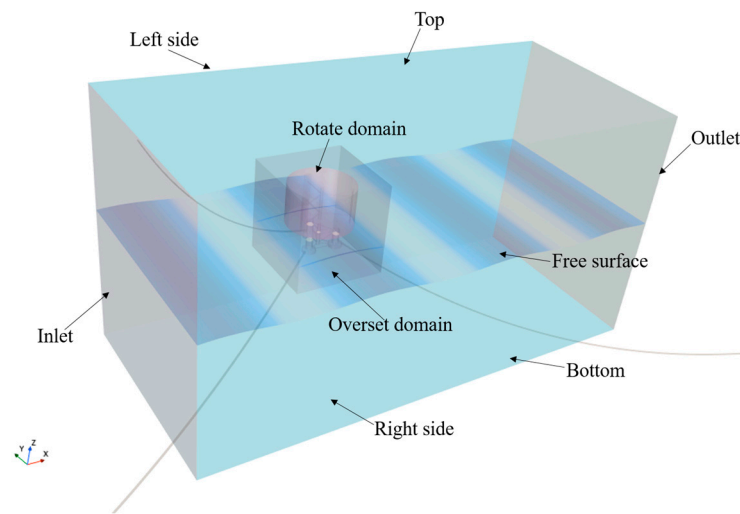


Figure 8. Computational domain and boundary.

According to the deep-sea environment, in the numerical tank, the boundary conditions on both two sides and bottom are symmetry, and the top and outlet are pressure outlets. Particularly, the inlet is a velocity inlet where wind and wave are produced. To avoid the potential error induced by drastic motion, the whole system-body free motion domain is filled with overset mesh, and the outline surface of this domain is overset. Additionally, rotating motion is achieved by applying the entire rotate domain to a constant angular velocity, and its outline surface is symmetric.

In addition, to produce a fully-developed wave-wind field, the distance between the velocity inlet and the model is greater than twice the length of the floating structure. While, the distance between the outlet and the model is more than four times the length of the floating structure to consider the effect of wake, especially gas wake. In addition, the distance between the sides and the model is similar to the strategy of velocity inlet. The distance between the top and the model is larger than the rotor height, and the distance between the bottom and the model is greater than twice the platform height.

4.4.2. Strategy and Convergence of Mesh

In the process of meshing, trim and prisms layer mesh generators are used to produce the volume mesh; volume and surface control techniques are combined for mesh refinement. Smaller mesh size is helpful to capture tiny details in the fluid domain, however, it means the computational resource requirement will increase rapidly. Thus, a suitable meshing strategy gives considerations to both accuracy and computational cost.

Figure 9 demonstrates the meshing strategy adopted in this paper by showing a longitudinal section. Modeling the wave shape precisely is essential as wave load is the main contributor to the hydrodynamic load, the entire wave propagation region is contained by the free surface domain. Therefore, using volume control technology refines the mesh in both wave length (x) and wave height (z) directions. In addition, it is also necessary to refine the mesh in wake area as the uniform wind is disturbed significantly after flowing through the rotating rotor. Attentionally, to ensure successful mesh interpolation, the mesh size near the interface between the overset and background domains should be closer, as well as the interface between the overset and sliding domains.

The mesh-independent analysis is required to determine the mesh size under a certain computational model and mesh strategy. The OF-VAWT system in this study will be affected by both uniform wind and regular waves, so there is a complex gas-liquid two-phase domain and energy dissipation during wind-wave propagation. Therefore, the mesh-independent analysis is conducted by checking wave shape. The grids are divided into three types named Mesh1, Mesh2 and Mesh3 according to the difference in the basic size, and the total number of grids are 540, 902 and 1415 million, respectively. Then, wave

results of three meshing types are compared with the theoretical values, respectively, and the fully-developed wave results are shown in Figure 10. It is clear that the magnitude of Mesh1 has a large difference from the theoretical value, and there is an obvious phase difference. The results of Mesh2 and Mesh3 are closer to the theoretical value, and the results are acceptable, but the number of meshes of Mesh3 is significantly larger than that of Mesh2. Therefore, Mesh2 is selected as the final grid strategy in this paper, and the total number of grids is 902 million.

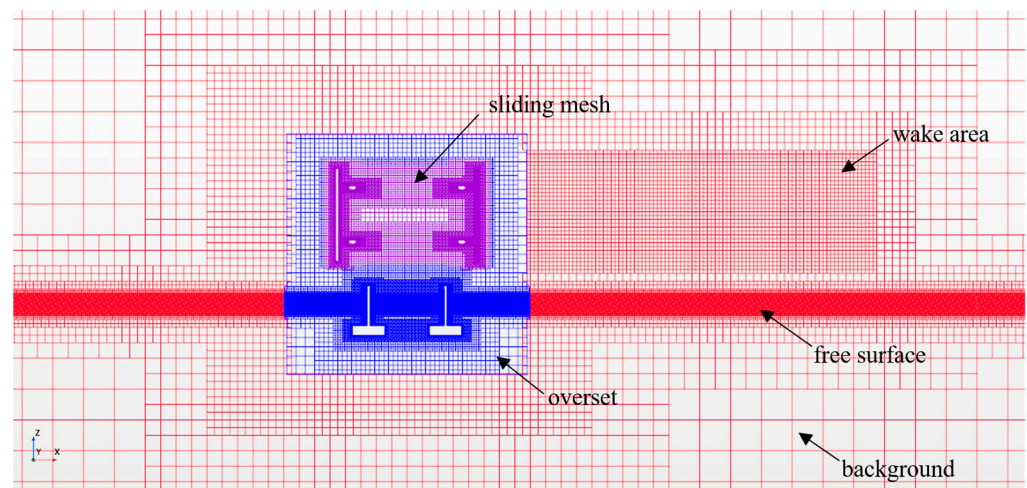


Figure 9. Grid partitioning strategy in longitudinal section.

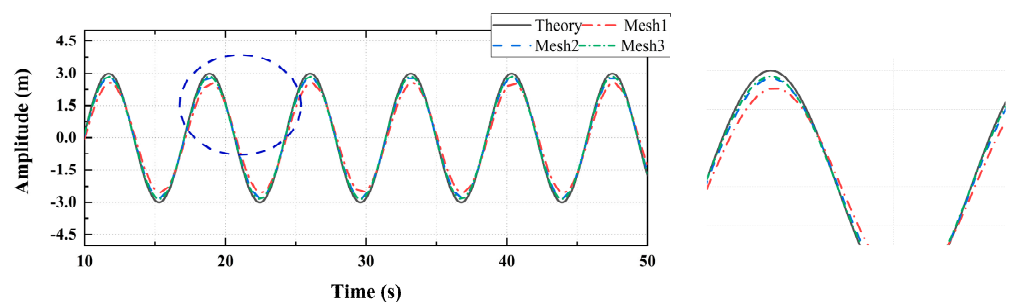


Figure 10. Time-domain wave-making amplitude curve of different mesh type.

4.4.3. Simulation Case

To find the TSR with optimal performance, analyzing the aerodynamic performance of the VAWT separately is essential and then integrating it into the OF-VAWT system. In addition, the VAWT in this paper is the full-scale experimental model [26], and it suffers from tower shadow effect, the same as other HAWTs [31], so the aerodynamic performance reduction is studied briefly. By applying present aerodynamic module, the power and torque coefficients with and without the tower at different TSR are acquired and shown in Figure 11. Obviously, the tower shadow effect makes the value decrease with different degrees, and the reduction is more obvious as the TSR increases. More importantly, the optimal performance of this rotor appears when TSR is approximately 1.75.

To ensure that the rotor is performing well at most times, the rotational speed is determined by optimal TSR of 1.75 in all general cases, including under different wind speed. It is well-known that wave height, wave length, wind speed and propagation direction are the main environmental parameters. However, it can be noticed the inertia of this OF-VAWT model is equal in both the X and Y directions (Table. 3), which means similar motion response in both directions. Thus, the propagation direction of wind-wave is not considered and specified in the X-positive direction.

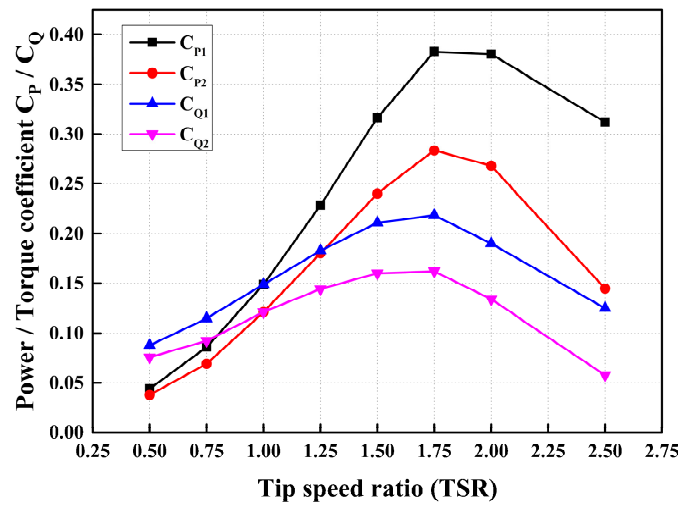


Figure 11. Power and torque coefficient of rotor with tower C_{P1} , C_{Q1} and without tower C_{P2} , C_{Q2} .

By referring to the statistics of the South China Sea, it is clear that the average wave height is 6 m and the wind speed is 20 m/s. To investigate the load and performance in different wave height, four cases including GC.1, GC.2, GC.3 and GC.4 are carried out in which wave height is from 2 m to 10 m. We also present five cases to study the effect of different wave length including GC.5, GC.3, GC.6, GC.7 and GC.8. Similarly, the effect of wind speed is considered by conducting four cases including GC.9, GC.10, GC.3 and GC.11. Additionally, it is common that extreme environments may appear suddenly when offshore structures are operating, so two extreme cases are added to compare with general cases. The cases are listed in Table 6.

Table 6. General and extreme cases of OF-VAWT in wind-wave coupling environment.

Case	H (m)	λ/L	V_∞ (m/s)
GC.1	2	1	20
GC.2	4	1	20
GC.3	6	1	20
GC.4	10	1	20
GC.5	6	0.75	20
GC.6	6	1.25	20
GC.7	6	1.5	20
GC.8	6	2	20
GC.9	6	1	10
GC.10	6	1	15
GC.11	6	1	30
EC.1	7.5	-	40
EC.2 (parked)	14	-	60

5. Time-Domain Analysis

Aero-hydrodynamic load and performance in general and extreme cases are obtained by applying the numerical model proposed in this paper. Previous related research mainly concentrates on characteristics in frequency-domain by establishing simplified models [20]. Hence, it is necessary to investigate the time-domain characteristics in typical wind-wave environments before statistical analysis, the time-domain data of GC.3, EC.1 and EC.2 will be presented in this section.

Figure 12 shows the operating state of OF-VAWT including distributions of wind velocity and wave elevation. Obviously, the wave-field near the platform is disturbed slightly and generates reflection, radiation and run-up. Furthermore, there is a significant velocity reduction zone after wind flow through the rotor.

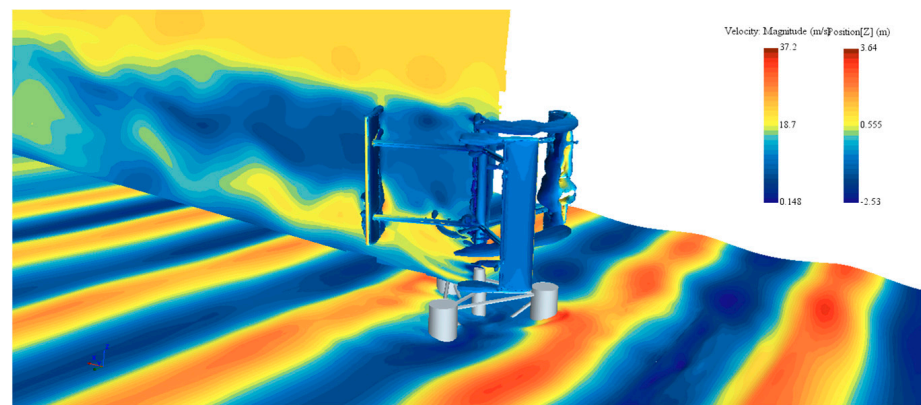


Figure 12. The operating OF-VAWT in the gas-liquid flow field of case 3.

The time-domain forces and bending moments of the axial and lateral directions in a general case are given in Figure 13. Axial thrust attracts more concerns in related works of HAWT [32], however, this VAWT generates the obvious lateral load although axial loads generated by the rotating rotor and platform are significantly greater than lateral loads in head wind-wave conditions, and the period of hydrodynamic load is more than twice of aerodynamics in axial direction while it is similar in lateral direction. More importantly, it is noted that the rotor force is far away from the mass central point. This may be the major reason why aerodynamic bending moment is the dominant component of the total bending moment although the aerodynamic force is relatively small compared to hydrodynamic force in both two directions. In a word, the effect of aerodynamic loads generated by rotor on floating systems presented in this part has implications for engineering design.

Considerable efforts have been made to study the effect of floating foundation motion on turbine aerodynamics in offshore FOWTs by many researchers. It indicates that the thrust and torque values are stable and nearly constant when HAWT is fixed [32,33]. This may be the reason why the aerodynamic frequency is close to motion frequency, such as pitch [34] and surge motion [30,35]. For VAWT, the oscillation of aerodynamics is significant. Cheng et al. [36] noted that the aerodynamic value of two-bladed VAWT varies from zero to twice mean value in a period and revealed the two-peak characteristics. However, the aerodynamics of three-bladed VAWT in this paper is not significantly disturbed by motion on period except for slight fluctuations in amplitude. Figure 14 shows the aerodynamic performance curves in one period, it is evident that the main power of a single blade is generated in the upwind area with a single-peak phenomenon. As a result, the three-peak characteristic of total torque curve is produced due to the sequential passed three blades. Thus, improving the performance in downwind area could be a feasible way to promote application of VAWT.

To date the existing works that can consider the aero- hydrodynamics of FOWT mainly adopted the way modeling and integrating each simplified module, respectively, including FloVAWT [37], HAWC2 [38], SIMO-RIFLEX-AC [36], and SIMO-RIFLEX-DMS [22]. However, the characteristics in frequency-domain are the major concentration due to its limitation in theory. To reveal the performance difference in general and extreme environments, torque, pitch and heave motion are compared in time-domain, as shown in Figure 15. Obviously, the aerodynamic torque peak of operating rotor in EC.1 is larger than twice it in GC.3. However, the expectation of torque reduction does not appear by stopping operation of the rotor in EC.2, and the average, as well as peak and valley, are more serious. The results indicate that the aerodynamic load of the OF-VAWT should be reduced by adding control module adjusting the pitch angle under extreme cases. In addition, motions such as pitch and heave are more violent when wind speed and wave height are larger. Further, two pictures (see Figure 16) are given to demonstrate the floating state in the two extreme environments. In the EC.1 case, the sea level is close to up-deck of OF-VAWT due to obvious pitch motion, and there is a long distinct zone of velocity reduction induced by

the operating rotor in air domain. For worse conditions (EC.2), the whole deck is almost submerged under violent pitch motion and rough seas. There is still an obvious decrease in wind speed due to resistance induced by stationary rotor, but with a smaller zone.

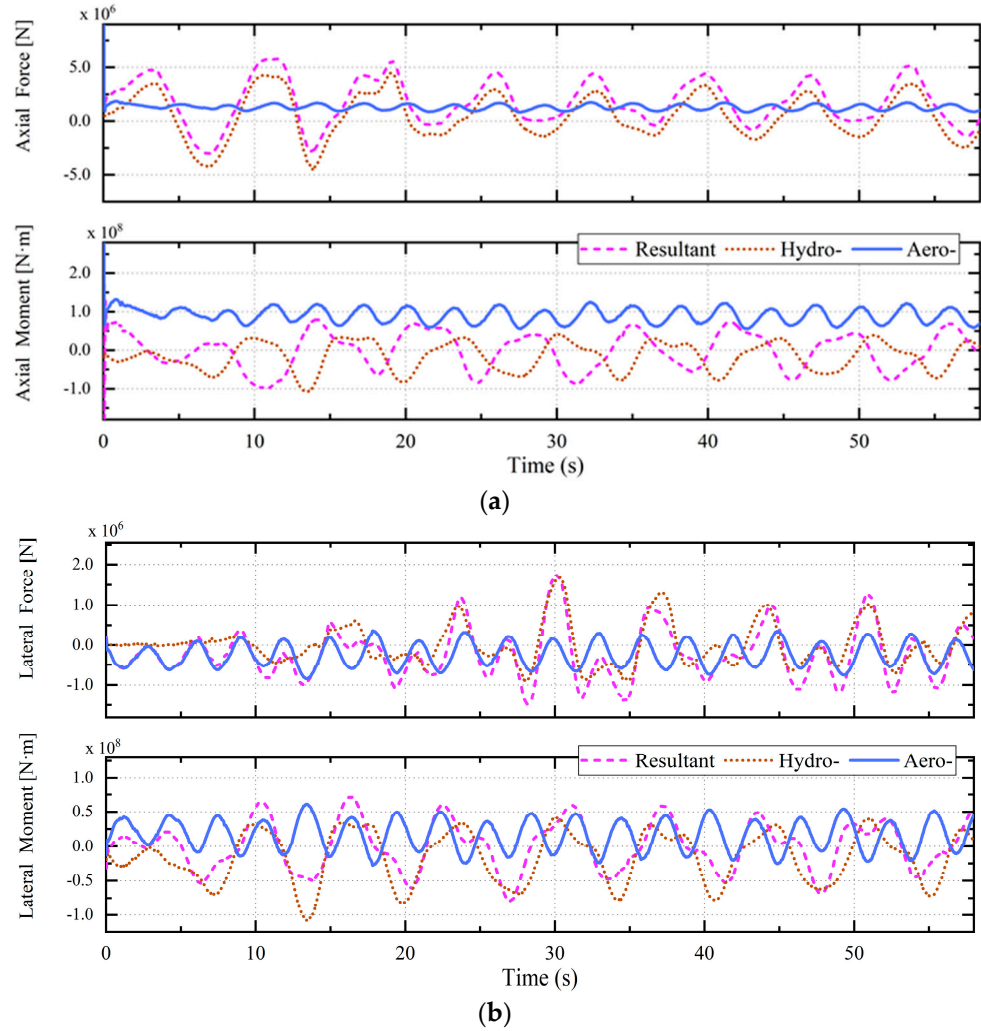


Figure 13. Time–domain curve of aero–hydrodynamic force and bending moment in case 3: (a) Axial force and bending moment (X–axes); (b) Lateral force and bending moment (Y–axes).

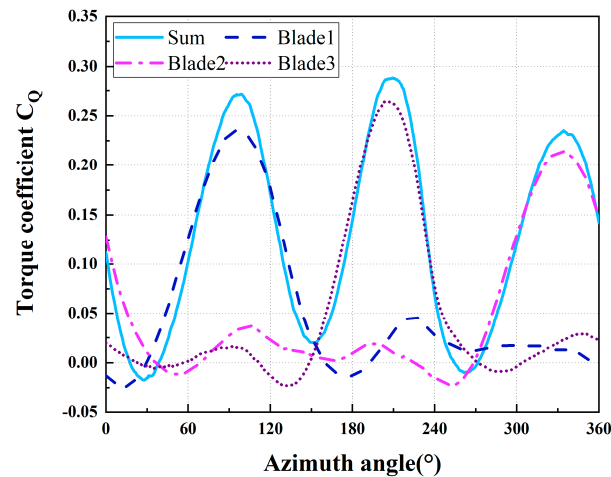


Figure 14. Time–domain curve of aerodynamic performance with azimuth angle in case 3.

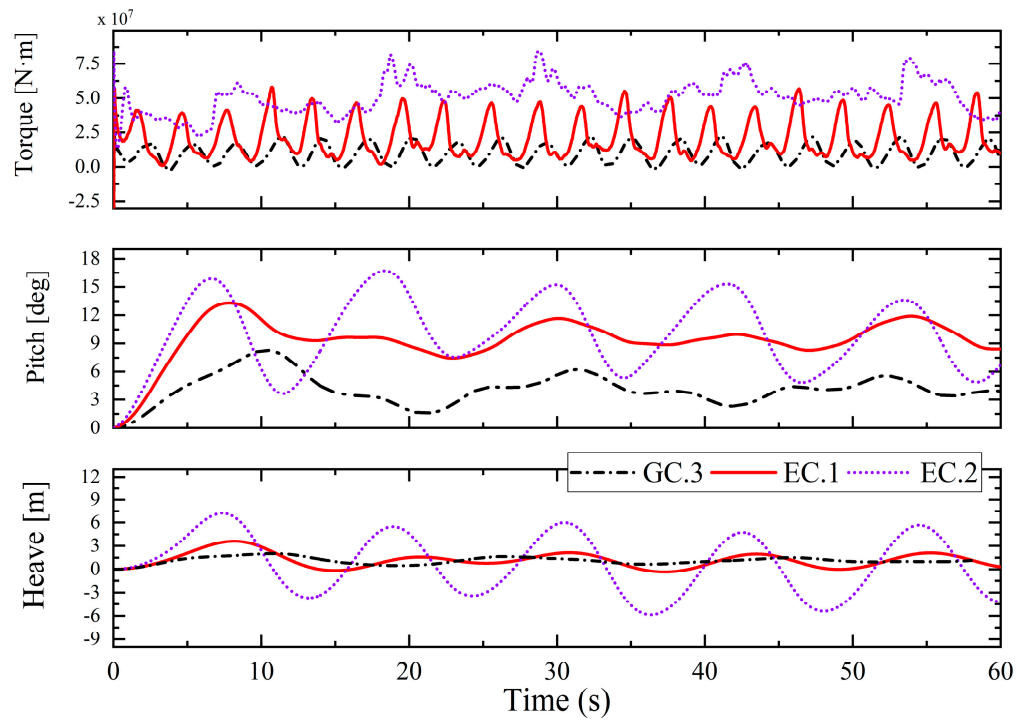


Figure 15. Time-domain curve of aerodynamic performance and hydrodynamic motion in case 3.

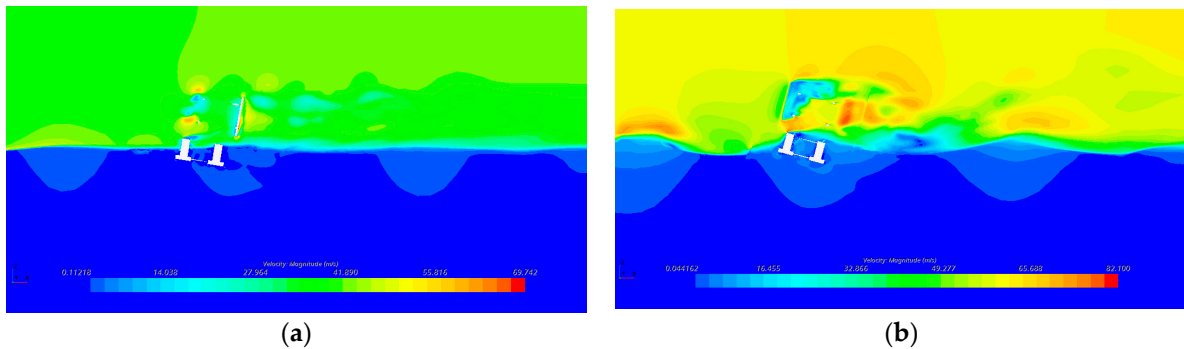


Figure 16. Floating state of OF-VAWT in extreme cases: (a) EC.1; (b) EC.2.

6. Discussion

The load and performance characteristics in time-domain were analyzed in the previous section, particularly, the aerohydrodynamic load attract attention from structural safety and survival. Some researchers have conducted a series of wind-wave cases investigating the OF-VAWT performance [39,40], but the effect of each environmental variable has not yet been concluded. In this section, we compared the differences in motions and power under different cases to discuss the effect of environmental parameters, including wave height, wave length and wind speed, on OF-VAWT performance.

Wave height as an important part of the wave parameters represents the elevation of the wave peak from the wave valley, the wave shape is steeper as the wave height increases. Figure 17 shows the statistics for variable wave height cases, mean and standard deviation (STD) values are combined to analyze the trend and destabilization of data. Obviously, the pitch motion is always significant compared to heave and roll, and roll motion increased rapidly in extreme environments although it is negligible in general cases. The motion mean value increases with wave height, especially for pitch motion, and the amplitude range of all motion grows with wave height by observing the STD. In addition, there is a slight reduction of the power coefficient when wave height increases, particularly, the power coefficient in extreme cases is unacceptable.

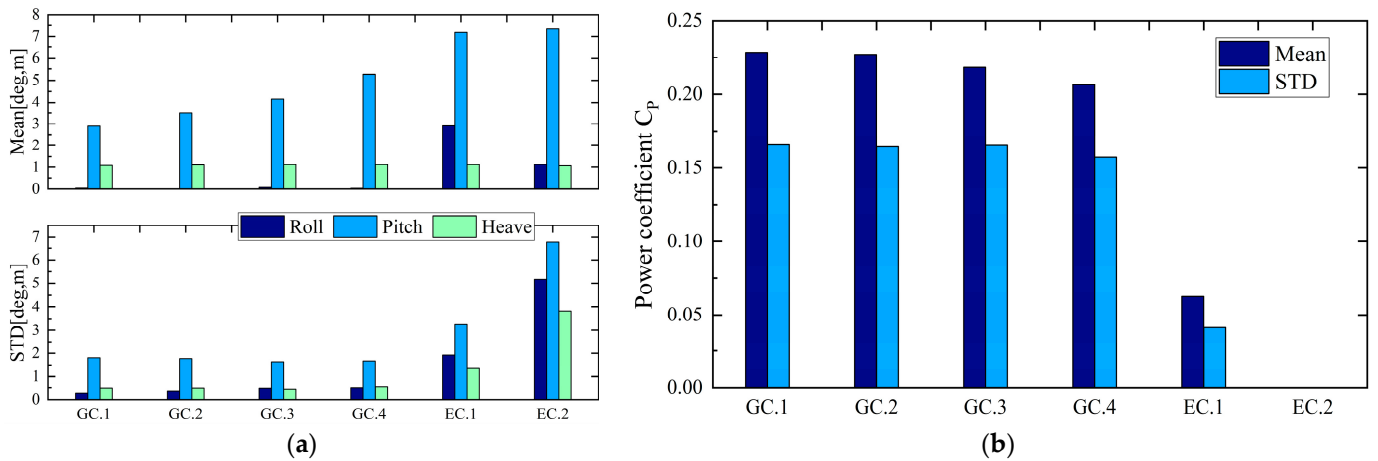


Figure 17. Aero-hydrodynamic performance in variable wave height case: (a) Mean and STD value of motion response; (b) Mean and STD value of power coefficient.

Similarly, wave length represents the distance between two wave peaks, the wave shape is smoother as the wave length increases. By analyzing Figure 18, it is obvious that the motions increase first and then decrease in general cases, however, the STD is of a slight difference. The trend of power coefficient is opposite to motion in variable wave length cases. Attentionally, the mean value of both motion and power have obvious changes induced by wave, but the STD value is stable. However, both of them are susceptible to an extreme environment.

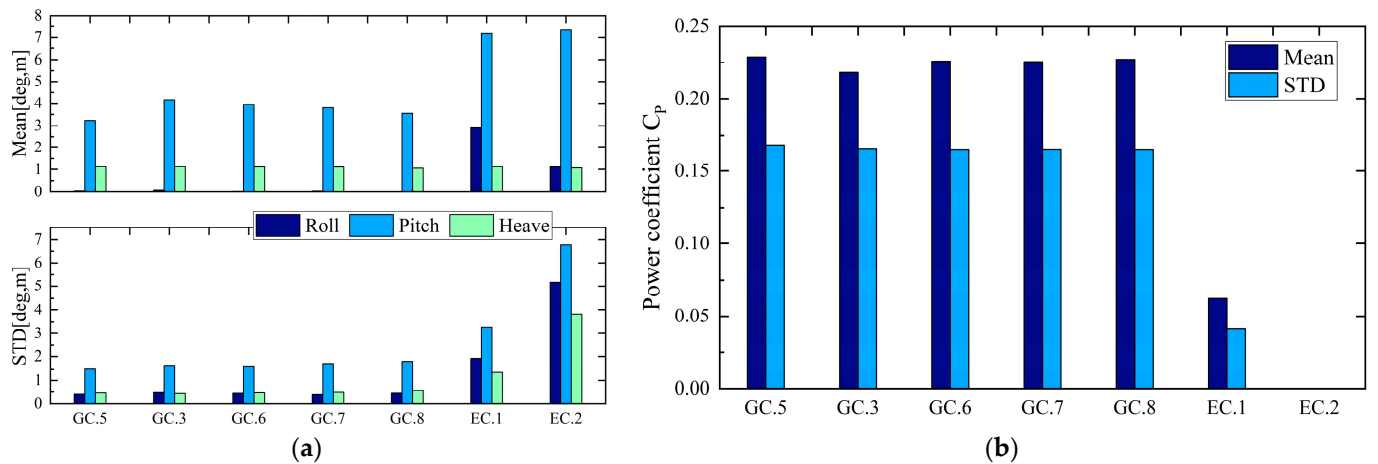


Figure 18. Aero-hydrodynamic performance in variable wave length case: (a) Mean and STD value of motion response; (b) Mean and STD value of power coefficient.

The wind speed indicating wind strength is important to influence aerodynamics. Figure 19 shows the motion and power at different wind speeds. Different from wave impact, it is obvious that both mean and STD values of motion increase rapidly with wind speed, and the amplitude of motion is more susceptible to wind than waves, for example, the max mean value of pitch in general wind speed cases is approximately 7 degrees, while it is 5 degrees in general wave cases. Furthermore, the power coefficient is in decline with increased wind speed, and the maximum reduction of power coefficient induced by wind speed is significant compared to it induced by waves. However the STD is relatively independent of wind speed in general cases.

It is obvious that there is a large difference in motion and in the power of extreme cases and general cases. With wave height or length increases, the maximum mean value of motion in general cases is merely two-thirds of it in extreme cases. However, this value in

general wind speed cases is close to extreme cases. A similar pattern appears in the power coefficient variation. This comparison indicates that wind speed is more crucial than wave parameters to the OF-VAWT system. In addition, extreme environments change both the mean and STD value apparently, especially for power coefficient. For instance, the pitch motion in extreme cases is approximately 7.5 degrees while it is approximately 4 in general cases. Particularly, the power coefficient in extreme cases is only 0.075, which means the wind generator is not effective any longer.

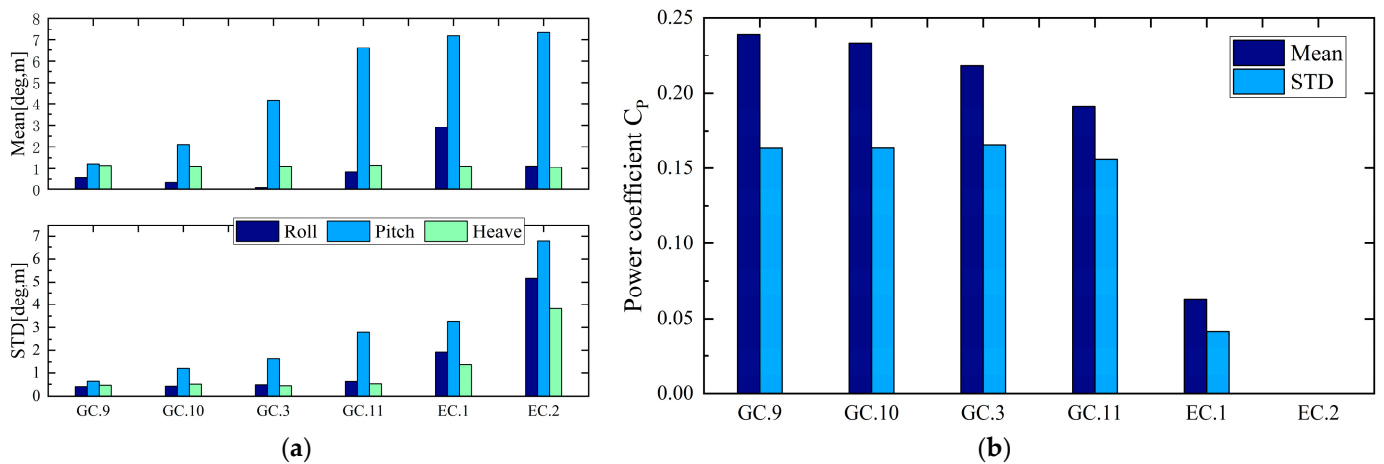


Figure 19. Aero-hydrodynamic performance in variable wind speed case: (a) Mean and STD value of motion response; (b) Mean and STD value of power coefficient.

Researchers found that VAWTs perform better in wind farms considering wake effect [41]. Further, it is noted that several offshore VAWTs were developed or produced recently, such as 1MW-S2x designed by SeaTwirl and 30kW-S1 operated in Lysekil. However, these products or concepts are mainly developed for tests and validation, and almost no floating VAWTs for deep sea exist. Therefore, the findings in this paper reveal the physics in advance and have implications for designing OF-VAWTs in the future.

It is worth noting that the prediction of aero-hydrodynamics using CFD is accurate and reliable, however, the time cost is a trouble for promotion and application. Therefore, there are still challenges for VAWT development. For instance, the detailed analysis in aerodynamics is important for VAWT improvement, such as dynamics stall effect [42–45]. Some scholars have also considered small VAWT development [46]. To balance the time cost and accuracy, researchers proposed and improved aerodynamic models for VAWT, such as double-multiple streamtubes [47,48]. These fields are still the key point in VAWT in the future.

7. Conclusions

In this study, a numerical model of OF-VAWT considering aero-hydro-mooring dynamics was developed by combining CFD technology, DFBI superposition motion method and the catenary model. First, the validation of this method was conducted by comparing the aero-hydrodynamic data with two model experiments, respectively. Then, the time-domain load and performance of OF-VAWT in both general and extreme environments were presented and analyzed. Finally, we discussed the performance distributions with different environmental parameters by the statistics and compared them with extreme responses. Several conclusions were obtained as follows.

1. The aerodynamic bending moment is always dominant in a total bending moment, and the aerodynamic torque induced by rotor resistance in extreme environments is significant. These results indicate that OF-VAWT has the requirement for a control module adjusting the pitch angle under extreme cases to reduce aerodynamic loads although VAWT has the ability to harness the energy in each direction without steering.

2. In a wind-wave environment, the trend of power coefficient is opposite to motion. The performance variation is different in each case, quantitative analysis indicates the performance of OF-VAWT is more susceptible to wind compared to waves.
3. In extreme environments, the power coefficient generated by rotors is unacceptable under a violent motion, nearly a quarter of the normal. In addition, there is severe green water induced by violent motion in enormous waves, and even the deck is almost submerged in the worst condition.

In this paper, we concluded the loads and performance of straight-blade OF-VAWT in both general and extreme environments; a comparison shows that OF-VAWT is more susceptible to wind speed than waves. The findings of this study have implications for engineering design. However, the present work concentrates on aero-hydrodynamic performance, and the structural responses are not considered, thus related fluid–structure interaction research will be conducted in the future.

Author Contributions: W.L. (Wenping Luo): simulation, validation, writing—original draft, writing—review and editing, visualization; W.L. (Weiqin Liu): funding acquisition, supervision, methodology; M.Y.: supervision, methodology; S.C.: investigation, data curation, software, information retrieval; X.S.: supervision, methodology; W.W.: supervision, methodology. All authors have read and agreed to the published version of the manuscript.

Funding: This research was funded by the National Natural Science Foundation of China (No.: 52071243, 52101371) and the National Defense Basic Research Program of China (No.: JCKY2020206B037).

Institutional Review Board Statement: Not applicable.

Informed Consent Statement: Not applicable.

Data Availability Statement: The data is in the article.

Conflicts of Interest: The authors declare no conflict of interest.

References

1. Kaldellis, J.K.; Apostolou, D.; Kapsali, M.; Kondili, E. Environmental and social footprint of offshore wind energy. comparison with onshore counterpart. *Renew. Energy* **2016**, *92*, 543. [\[CrossRef\]](#)
2. Ismail, M.F.; Vijayaraghavan, K. The effects of aerofoil profile modification on a vertical axis wind turbine performance. *Energy* **2015**, *80*, 20–31. [\[CrossRef\]](#)
3. Borg, M.; Collu, M.; Kolios, A. Offshore floating vertical axis wind turbines, dynamics modelling state of the art. part ii: Mooring line and structural dynamics. *Renew. Sustain. Energy Rev.* **2014**, *39*, 1226–1234. [\[CrossRef\]](#)
4. Rosenthal, W.; Lehner, S. Rogue waves: Results of the maxwave project. *J. Offshore Mech. Arct. Eng.* **2008**, *130*, 21006. [\[CrossRef\]](#)
5. Chou, J.S.; Chiu, C.K.; Huang, I.K.; Chi, K.N. Failure analysis of wind turbine blade under critical wind loads. *Eng. Fail. Anal.* **2013**, *27*, 99–118. [\[CrossRef\]](#)
6. Zhang, X.; Wang, M.; Wang, Y.; Liu, Y. Research on Failure of Offshore Wind Turbine Tower in Typhoon. In Proceedings of the 2018 OCEANS-MTS/IEEE Kobe Techno-Oceans (OTO), Kobe, Japan, 28–31 May 2018.
7. Lechuga, A. Were freak waves involved in the sinking of the tanker “prestige”? *Nat. Hazards Earth Syst. Sci.* **2006**, *6*, 973–978. [\[CrossRef\]](#)
8. Su, J.; Li, Y.; Chen, Y.; Han, Z.; Zhou, D.; Zhao, Y.; Bao, Y. Aerodynamic performance assessment of ϕ -type vertical axis wind turbine under pitch motion. *Energy* **2021**, *225*, 1. [\[CrossRef\]](#)
9. Lei, H.; Zhou, D.; Bao, Y.; Chen, C.; Ma, N.; Han, Z. Numerical simulations of the unsteady aerodynamics of a floating vertical axis wind turbine in surge motion. *Energy* **2017**, *127*, 1. [\[CrossRef\]](#)
10. Lei, H.; Zhou, D.; Lu, J.; Chen, C.; Han, Z.; Bao, Y. The impact of pitch motion of a platform on the aerodynamic performance of a floating vertical axis wind turbine. *Energy* **2017**, *119*, 369. [\[CrossRef\]](#)
11. Wu, J.; Meng, L.; Zhao, Y.; He, Y. Coupled aerodynamic and hydrodynamic analysis of floating offshore wind turbine using cfd method. *Trans. Nanjing Univ. Aeronaut. Astronaut.* **2016**, *33*, 80–87.
12. Tran, T.T.; Kim, D.H. A cfd study of coupled aerodynamic-hydrodynamic loads on a semisubmersible floating offshore wind turbine. *Wind Energy* **2018**, *21*, 70–85. [\[CrossRef\]](#)
13. Wang, H.; Hu, Z.Q.; Meng, X.Y. Dynamic performance investigation of a spar-type floating wind turbine under different sea conditions. *China Ocean Eng.* **2018**, *32*, 256–265. [\[CrossRef\]](#)
14. Zhang, Y.; Kim, B. A fully coupled computational fluid dynamics method for analysis of semi-submersible floating offshore wind turbines under wind-wave excitation conditions based on oc5 data. *Appl. Sci.* **2018**, *8*, 2314. [\[CrossRef\]](#)

15. Guo, Y.; Liu, L.Q.; Li, Y.; Xiao, C.S.; Tang, Y.G. The surge-heavepitch coupling motions of the ϕ -type vertical axis wind turbine supported by the truss spar floating foundation. *J. Hydrodyn.* **2019**, *31*, 669–681. [[CrossRef](#)]
16. Cheng, P.; Huang, Y.; Wan, D. A numerical model for fully coupled aero-hydrodynamic analysis of floating offshore wind turbine. *Ocean Eng.* **2019**, *173*, 183–196. [[CrossRef](#)]
17. Li, X.; Zhu, C.; Fan, Z.; Chen, X.; Tan, J. Effects of the yaw error and the wind-wave misalignment on the dynamic characteristics of the floating offshore wind turbine. *Ocean Eng.* **2020**, *199*, 106960. [[CrossRef](#)]
18. Gao, J.; Griffith, D.T.; Sakib, M.S.; Boo, S.Y. A semi-coupled aeroservo-hydro numerical model for floating vertical axis wind turbines operating on ttps. *Renew. Energy* **2022**, *181*, 692–713. [[CrossRef](#)]
19. Lee, H.; Poguluri, S.K.; Bae, Y.H. Development and verification of a dynamic analysis model for floating offshore contra-rotating vertical axis wind turbine. *Energy* **2022**, *240*, 122492. [[CrossRef](#)]
20. Borg, M.; Shires, A.; Collu, M. Offshore floating vertical axis wind turbines, dynamics modelling state of the art. part i: Aerodynamics. *Renew. Sustain. Energy Rev.* **2014**, *39*, 1214–1225. [[CrossRef](#)]
21. Liu, L.; Guo, Y.; Zhao, H.; Tang, Y. Motions of a 5 mw floating vawt evaluated by numerical simulations and model tests. *Ocean Eng.* **2017**, *144*, 21–34. [[CrossRef](#)]
22. Wang, K.; Hansen, M.O.L.; Moan, T. Dynamic analysis of a floating vertical axis wind turbine under emergency shutdown using hydrodynamic brake. *Energy Procedia* **2014**, *53*, 56–69. [[CrossRef](#)]
23. Vita, L. Offshore Floating Vertical Axis Wind Turbines with Rotating Platform. Ph.D. Thesis, Technical University of Denmark (DTU), Denmark, 2011.
24. Jin, X.; Zhao, G.; Gao, K.; Ju, W. Darrieus vertical axis wind turbine: Basic research methods. *Renew. Sustain. Energy Rev.* **2015**, *42*, 212–225. [[CrossRef](#)]
25. Bianchini, A.; Balduzzi, F.; Ferrara, G.; Ferrari, L.; Persico, G.; Dossena, V.; Battisti, L. Detailed analysis of the wake structure of a straight blade h-darrieus wind turbine by means of wind tunnel experiments and computational fluid dynamics simulations. *J. Eng. Gas Turbines Power* **2018**, *140*, 32604. [[CrossRef](#)]
26. Maeda, T.; Kamada, Y.; Murata, J.; Furukawa, K.; Yamamoto, M. Effect of number of blades on aerodynamic forces on a straight-bladed vertical axis wind turbine. *Energy* **2015**, *90*, 784.
27. Coulling, A.J.; Goupee, A.J.; Robertson, A.N.; Jonkman, J.M.; Dagher, H.J. Validation of a fast semi-submersible floating wind turbine numerical model with deepcwind test data. *J. Renew. Sustain. Energy* **2013**, *5*, 23116. [[CrossRef](#)]
28. Tran, T.T.; Kim, D.H. The coupled dynamic response computation for a semi-submersible platform of floating offshore wind turbine. *J. Wind Eng. Ind. Aerodyn.* **2015**, *147*, 104–119. [[CrossRef](#)]
29. Luan, C.; Gao, Z.; Moan, T. Modelling and Analysis of a Semi-Submersible Wind Turbine with a Central Tower with Emphasis on the Brace System. In Proceedings of the Asme International Conference on Ocean, Nantes, France, 9–14 June 2013.
30. Tran, T.T.; Kim, D.H. A cfd study into the influence of unsteady aerodynamic interference on wind turbine surge motion. *Renew. Energy* **2016**, *90*, 204–228. [[CrossRef](#)]
31. Mohammadi, E.; Fadaeinedjad, R.; Naji, H.R. Using a new wind turbine emulator to analyze tower shadow and yaw error effects. *Energy Convers. Manag.* **2018**, *174*, 378–387. [[CrossRef](#)]
32. Huang, Y.; Cheng, P.; Wan, D. Numerical analysis of a floating offshore wind turbine by coupled aero-hydrodynamic simulation. *J. Mar. Sci. Appl.* **2019**, *18*, 82. [[CrossRef](#)]
33. Borg, M.; Collu, M. A comparison between the dynamics of horizontal and vertical axis offshore floating wind turbines. *Philos. Trans. R. Soc. A: Math. Phys. Eng. Sci.* **2015**, *373*, 20140. [[CrossRef](#)]
34. Fang, Y.; Duan, L.; Han, Z.; Zhao, Y.; Yang, H. Numerical analysis of aerodynamic performance of a floating offshore wind turbine under pitch motion. *Energy* **2020**, *192*, 116. [[CrossRef](#)]
35. Farrugia, R.; Sant, T.; Micallef, D. A study on the aerodynamics of a floating wind turbine rotor. *Renew. Energy* **2016**, *86*, 770–784. [[CrossRef](#)]
36. Cheng, Z.; Madsen, H.A.; Gao, Z.; Moan, T. A fully coupled method for numerical modeling and dynamic analysis of floating vertical axis wind turbines. *Renew. Energy* **2017**, *107*, 604. [[CrossRef](#)]
37. Collu, M.; Borg, M.; Shires, A.; Brennan, F.P. FloVAWT: Progress on the development of a coupled model of dynamics for floating offshore vertical axis wind turbines. In Proceedings of the International Conference on Offshore Mechanics and Arctic Engineering, American Society of Mechanical Engineers, Nantes, France, 9–14 June 2013; p. V008T09A045.
38. Larsen, T.J.; Madsen, H.A. On the way to reliable aeroelastic load simulation on vawts. *Proc. EWEA* **2013**, *9*, 2013.
39. Cheng, Z.; Wang, K.; Gao, Z.; Moan, T. A comparative study on dynamic responses of spar-type floating horizontal and vertical axis wind turbines. *Wind Energy* **2017**, *20*, 305–323. [[CrossRef](#)]
40. Cheng, Z.; Wang, K.; Gao, Z.; Moan, T. Dynamic response analysis of three floating wind turbine concepts with a two-bladed Darrieus rotor. *J. Ocean Wind Energy* **2015**, *2*, 213–222. [[CrossRef](#)]
41. Hansen, J.T.; Mahak, M.; Tzanakis, I. Numerical modelling and optimization of vertical axis wind turbine pairs: A scale up approach. *Renew. Energy* **2021**, *171*, 1371–1381. [[CrossRef](#)]
42. Bangga, G.; Hutomo, G.; Wiranegara, R.; Sasongko, H. Numerical study on a single bladed vertical axis wind turbine under dynamic stall. *J. Mech. Sci. Technol.* **2017**, *31*, 261–267. [[CrossRef](#)]
43. Bangga, G.; Hutani, S.; Heramarwan, H. The Effects of Airfoil Thickness on Dynamic Stall Characteristics of High-Solidity Vertical Axis Wind Turbines. *Adv. Theory Simul.* **2021**, *4*, 2000204. [[CrossRef](#)]

44. Ferreira, C.S.; Bijl, H.; Van Bussel, G.; Van Kuik, G. Simulating dynamic stall in a 2D VAWT: Modeling strategy, verification and validation with particle image velocimetry data. *J. Phys. Conf. Ser.* **2007**, *75*, 012023. [[CrossRef](#)]
45. Buchner, A.J.; Soria, J.; Honnery, D.; Smits, A.J. Dynamic stall in vertical axis wind turbines: Scaling and topological considerations. *J. Fluid Mech.* **2018**, *841*, 746–766. [[CrossRef](#)]
46. Bianchini, A.; Bangga, G.; Baring-Gould, I.; Croce, A.; Cruz, J.I.; Damiani, R.; Erfort, G.; Simao Ferreira, C.; Infield, D.; Nayeri, C.N.; et al. Current status and grand challenges for small wind turbine technology. *Wind Energy Sci.* **2022**, *7*, 2003–2037. [[CrossRef](#)]
47. Bangga, G.; Dessoky, A.; Lutz, T.; Krämer, E. Improved double-multiple-streamtube approach for H-Darrieus vertical axis wind turbine computations. *Energy* **2019**, *182*, 673–688. [[CrossRef](#)]
48. Paraschivoiu, I. Double-multiple streamtube model for studying vertical-axis wind turbines. *J. Propuls. Power* **1988**, *4*, 370–377. [[CrossRef](#)]

Disclaimer/Publisher’s Note: The statements, opinions and data contained in all publications are solely those of the individual author(s) and contributor(s) and not of MDPI and/or the editor(s). MDPI and/or the editor(s) disclaim responsibility for any injury to people or property resulting from any ideas, methods, instructions or products referred to in the content.